Deformation Analysis of Leonardo da Vinci's "Adorazione dei Magi" through Temporal Unrelated 3D Digitization

Gianpaolo Palma[a], Paolo Pingi[a], Eliana Siotto[a], Roberto Bellucci[b], Gabriele Guidi[c], Roberto Scopigno[a]

[a] *Visual Computing Lab - ISTI CNR, Pisa, Italy*
[b] *Opificio delle Pietre Dure, Florence, Italy*
[c] *Department of Mechanical Engineering, Politecnico di Milano, Italy*

Abstract

3D scanning is an effective technology for dealing at different levels the state of conservation/deformation of a panel painting, from the micro-geometry of the craquelure to the macro-geometry of the supported used. Unfortunately, the current solutions used to analyze multiple 3D scans acquired over time are based on very controlled acquisition procedures, such as the use of target reference points that are stationary over time and fixed to the artwork, or on complex hardware setups to keep the acquisition device fixed to the artwork. These procedures are challenging when a long monitoring period is involved or during restoration when the painting may be moved several times. This paper presents a new and robust approach to observe and quantify the panel deformations of artworks by comparing 3D models acquired with different scanning devices at different times. The procedure is based on a non-rigid registration algorithm that deforms one 3D model over the other in a controlled way, extracting the real deformation field. We apply the method to the 3D scanning data of the unfinished panel painting "Adorazione dei Magi" by Leonardo da Vinci. The data were acquired in 2002 and 2015. First, we analyze the two 3D models with the classical distance from the ideal flat plane of the painting. Then we study the type of deformation of each plank of the support by fitting a quadric surface. Finally, we compare the models before and after the deformation computed by a non-rigid registration algorithm. This last comparison enables the panel deformation to be separated from the structural changes (e.g. the structural restorations on the back and the missing pieces) of the artwork in a more robust way.

Keywords: 3D Digitization, Multi-temporal acquisition, Deformation analysis

1. Introduction

Monitoring the conservation state of a painting involves several aspects related to the support, the painted surface (preparation layers, subsequent paint layers, varnishes) and the protective coating. Several techniques are currently used to document the state of conservation of each of these components, such as imaging methods (Reflectance Transformation Imaging and Multi-spectral imaging), x-rays, 3D scanning, tomography, spectroscopy, acoustic imaging, and thermography. A painting, either on a canvas or on a wooden support, does not have a planar surface, but is in fact characterized by a complex multi-scale 3D shape, composed of the micro-geometry of the craquelure, the thickness of the painted surface and the macro-geometry of the support. All these geometric components may change over time due to the deformations induced by the conservation environment parameters (such as the positioning of the painting and the climate conditions). 3D scanning technologies facilitate the acquisition and documentation of this information.

In the analysis of an artwork during its restoration, the 3D documentation of the painted surface and its wooden support is extremely important. A panel painting is made up of a stratified structure with each layer having different physical and chemical characteristics. Therefore, an accurate 3D geometric model of the support and its connecting elements is fundamental for improving the knowledge of the artwork and its conservation status and for monitoring its status over time, particular during restoration.

This paper presents the results of the comparison of two 3D independent acquisitions of Leonardo da Vinci's unfinished masterpiece, the "Adorazione dei Magi", in order to evaluate how the panel has become deformed over time (Figure 1).

The "Adorazione dei Magi" measures about 2.44x2.40 meters with an average thickness of 4 cm. The painting was commissioned in 1481 by the friars of the convent of S. Donato in Scopeto (Florence) however it remained unfinished due to the Leonardo da Vinci's departure for Milan. The panel is composed of ten vertical poplar wooden planks of different widths (see right column in Figure 5 for the subdivision of the various planks). The planks are made of low-quality wood which are predisposed to deformations. They are predominantly sub-tangential/tangential, therefore tending to transversal cupping and shrinkage. The planks do not have internal connection elements and are held together by three

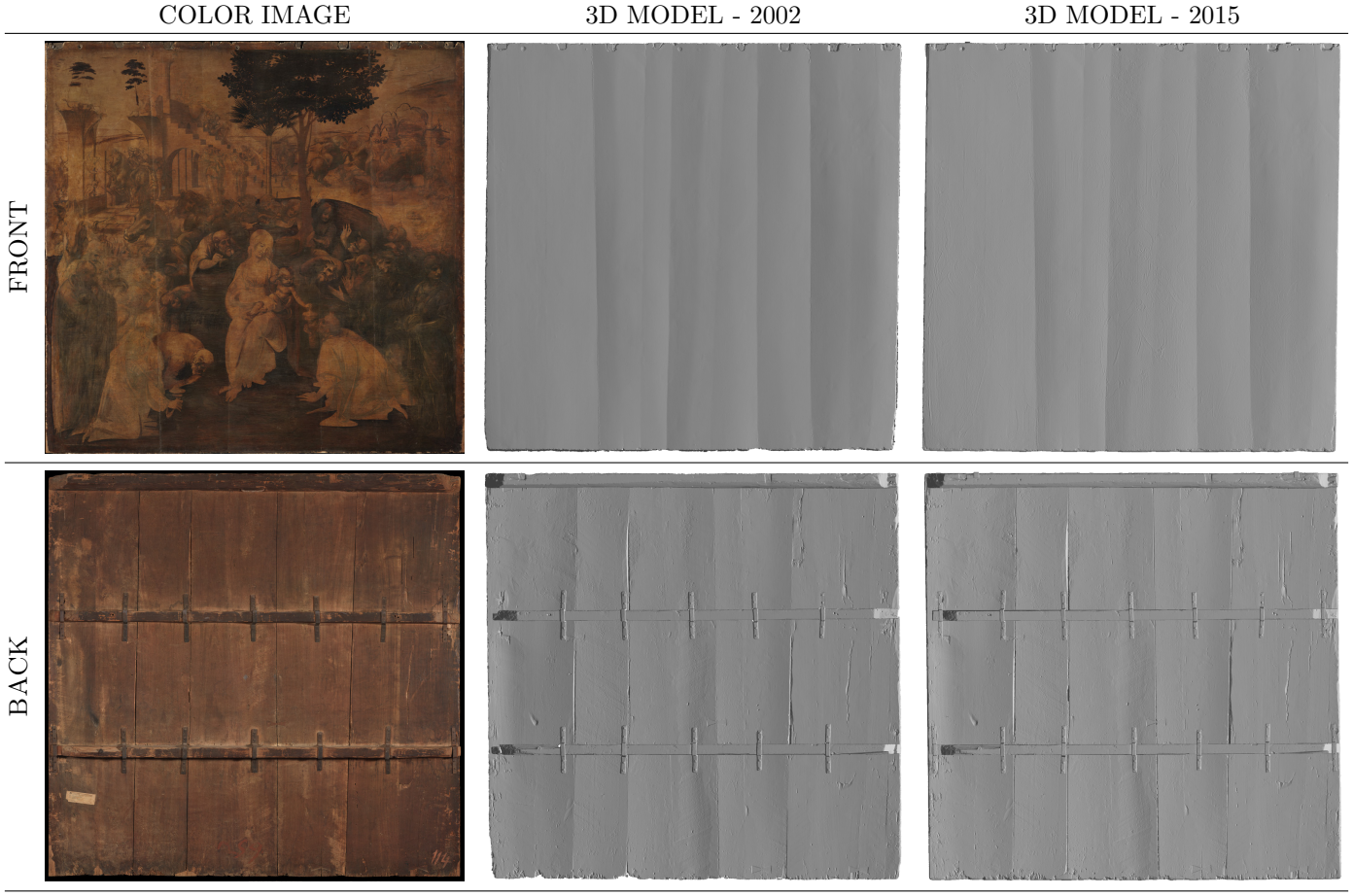

Figure 1: *Photos and 3D models of the two sides of the "Adorazione dei Magi" acquired in 2002 and in 2015.*

crossbars, one in the upper part and two in the central area (originally there was a fourth crossbar at the bottom which was removed). The crossbars are fastened to the panels with metal braces and nails (Figure 1). The planks were reinforced by several maple wood butterfly keys. A thick preparation layer (1.5-2mm), made with gypsum and glue, was laid on the front of the panel. Subsequently few shades of color were applied with an oil binder. At the border in the upper part of the panel, there are height pieces of wood of about 4/4.5 cm on each side. During the construction of the support, these pieces were removed and then put back in the same position before the preparation layer was laid.

Using the 3D models acquired in 2002 and 2015 with active 3D scanning technologies, first we analyzed the classical deformation from an ideal flat plane to assess the global distortion of the wooden support. Secondly, we studied the type of deformation of each plank using the fitting results of a quadric surface on the geometric data of the front side. Finally, we computed the real deformation between the two models through a non-rigid 3D registration in order to highlight and separate the low-frequency deformations from the new elements added to the support. The most common state-of-the-art approaches used for the evaluation of panel deformations are often based on very controlled and static acquisition environments in order to guarantee the correct alignment of the captured models over time. For example, the painting or the acquisition instruments need to stay in a fixed position throughout the monitoring period or stationary reference targets need to be placed directly over the artwork as control points in evaluating the deformation. This is very difficult when the monitoring period is long, especially during restoration when the painting may be moved several times or when targets points cannot be placed on the surface or it is not possible to ensure that they do not move. To overcome this problem we used a purely geometric approach which, using the data from two independent 3D acquisitions (in our case 13 years apart), computes the accurate deformation map without any assumption of the acquisition procedure used during the two 3D scanning campaigns. Using a non-rigid registration algorithm, which deforms one model to the other, it is possible to evaluate the real deformation and displacement of each point of the painting and robustly identify the most significant changes introduced by the different restorations over the years. Several structural elements were added, especially on the back of the painting, in order to make the panel more stable.

The results presented in this paper were used during the last restoration phase after 2015 in order to decide

how the wooden support should be structurally modified. In particular, we were able to check whether the structural changes introduced during the previous restoration between 2002 and 2015, had produced the right effects reducing the bowing deformation, and keeping cupping and twisting almost stable. From the results of this comparison, the restorers and conservators decided to carry out some interventions on the back of the support in order to further reduce the deformation, such as restoring the fourth crossbar at the bottom of the painting and modifying the three existing crossbars to reduce the stress on the ten planks. These results were then used to document the temporal evolution of the deformation of the support. For a complete review of the technical analysis and restoration of the wooden support, see [1] and in particular [2].

2. Research Aim

This paper presents a study of the panel deformation of Leonardo da Vinci's "Adorazione dei Magi" by comparing 3D models acquired with different scanning devices at different times. There are two main novelties in relation to this study. First is the fitting of a quadric surface on the geometric data of the planks in order to identify the different type of deformations. The second is the use of a non-rigid registration algorithm that deforms the 2002 model to the 2015 model in order to compute a smooth deformation field which is locally as rigid as possible. By comparing the models before and after the deformation computed by the non-rigid registration algorithm, we can extract and separate the information on the low-frequency deformation and the structural changes of the artwork (structural restorations and missing parts) in a more robust way. The proposed technique does not involve any strong requirements in the acquisition phase, such as the use of target reference points or a special acquisition setup to keep the position of the acquisition device fixed with respect to the artwork. It is based on independent 3D scanning acquisitions that are uncontrolled and unsupervised over time.

3. Related Work

For centuries wood was a common material used for supporting a painting, however it is prone to different types of degradation. A complete understanding of these deterioration processes is fundamental for correctly restoring and conserving a panel painting. A complete analysis of the most interesting research topics in this field is described in [3], together with a review of the techniques and methods used for the acquisition of information aimed at assisting the structural conservation of wooden panel paintings.

Many of these techniques document the state of the artwork in a single instance by combining several technologies that acquire different types of information. Maev et al. [4] review a number of techniques based on non destructive electromagnetic irradiation, such as: near-infrared imaging to reveal features hidden under or within the paint layers; thermography and scanning acoustic microscopy to evaluate the delamination of the wooden support; Raman spectroscopy to study the pigments; and optical coherence tomography to acquire information on the structure of the painted surface. Elias et al. [5] tested five different optical analyses (multispectral imaging, optical coherence tomography, goniophotometry, UV-fluorescence emission spectroscopy and diffuse reflectance spectroscopy) ans showed that the results of the different techniques were complementary and provided extensive information. Techniques based on holography interferometry [6] and digital speckle interferometry [7] detect surface defects while methods based on terahertz imaging ([8]), x-ray ([9]) and nuclear magnetic resonance ([10]) can be used to investigate the internal structure of the wooden support and to reveal subsurface features. Similarly, methods based on near-infrared light ([11] and [12]) investigate the painted surface and provide information on the hidden features, such as underdrawings and afterthoughts. On the other hand, the goal of methods based on 3D scanning is to compute a dense deformation field of the surface by comparing the 3D models with the ideal flat plane of the painting, as performed on the "Adorazione dei Magi" in [13]. Abate et al. [14] compared the accuracy obtained by two different 3D acquisition technologies, photogrammetry and structured light scanning. Comparing the distance between the two models from the ideal plane of the painting, they showed that the two techniques have a similar spatial accuracy. Remondino et al. [15] applied 3D scanning and multispectral imaging to assess the conservation state of paintings. Analysis of the 3D scanning data highlighted the deformation of the support, the brush strokes and color detachment on the painted surface. The challenge of integrating 3D data acquired by conoscopic micro-profilometry with the 2D data acquired by IR and color reflectography and UV digital fluorescence is discussed in [16]. Multispectral imaging for the study of painting is also proposed in [17].

A number of methods have been proposed to monitor and analyze artworks over time. Manfredi et al. [18] used of the Reflectance Transformation Imaging techniques to detect the morphological changes and damages (cracks, holes, and abrasion) on a painting by comparing the normal surface variations between the two acquisitions. Robson et al. [19] used photogrammetry techniques to monitor the deformation of a panel painting over several years using sparse stationary referenced points marked by retro-reflective targets fastened to the artwork. Similarly, Remondino et al. [15] employed targets placed on the canvas frame and acquired with a total station theodolite to establish a unique common reference system among different 3D acquisitions. Bratasz et al. [20] used a laser triangulation scanner for the on-site continuous monitoring of changes in a polychrome wooden altar over a two-year period. In this case, the acquisition device was kept stationary with respect to the object throughout the monitoring period.

An important aspect in investigating a panel painting is to assess the deformation caused by temperature and hu-

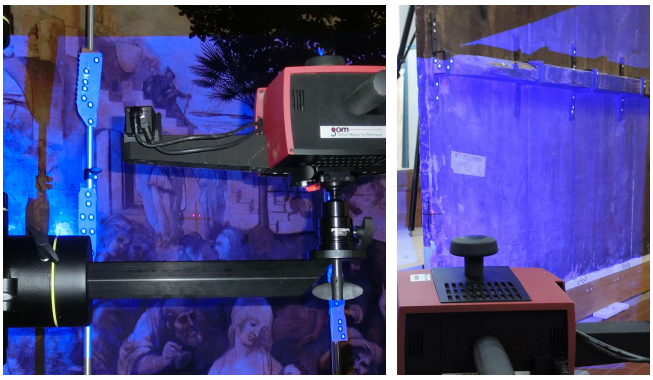

Figure 2: *Images of the acquisition of the front and back of the "Adorazione dei Magi" using the scanner ATOS Compact Scan 5M. The circular markers are positioned to automate the alignment of the range maps.*

midity. The most common technologies used to measure this deformation on a sample area are the Moiré fringe projection ([21], [22], and [23]) and the digital speckle interferometry ([24], [25], and [26]). Other solutions try to simulate this deformation in a laboratory, acquiring a section of a wooden panel treated in the same way as was standard for panel paintings in the past using a controlled climate chamber. Olstad et al. [27] investigated the deformation of a test piece using a grid of markers or drilled holes on the surfaces acquired by optical scanning. Dionisi-Vici et al. [28] used a mechanical device which, in contact with the test piece, measures cupping, swelling and shrinkage. The data acquired were then used to extract a mathematical model that highlights and predicts the deformations.

4. 3D Scanning Campaign

The "Adorazione dei Magi" was digitized at two different times with independent 3D scanning campaigns in different environmental conditions (humidity and temperature). The first one (2002, see [13]) was carried out in a warehouse at the Uffizi Museum, well before the planned restoration, in order to document the state of conservation of the painting. The second acquisition (2015) was performed at the "Opificio delle Pietre Dure" laboratory, when the artwork was already in an advanced state of cleaning. In the second acquisition, the aim was to give restorers a new 3D map of the deviations of the painted surface due to the curvature and deformations of the wooden support. The main purpose of the two acquisitions was to document the state of conservation at the time of scanning without any special procedures that enabling them to be compared with possible future acquisitions.

The first 3D acquisition campaign (2002) was performed with a structured light scanner designed and manufactured by Optonet ([29]), which consisted of a projector and a camera. Due to the impossibility of also scanning the border, two separated acquisitions were performed for the two sides of the painting at different times (a month apart): 393 scans were acquired for the front and 222 scans for the back. Each scan covers an area of 160 $\times$ 205 mm for the front and 205 $\times$ 269 for the back, with an overlap around the 30% with each adjacent scan. All the scans contain the color information that was used to simplify the alignment step. The alignment and merging steps of the scans were performed using IMAlign (Polyworks software suite [30]). The two final separate 3D models of the front and the back are composed of 13 and 10 million triangles with a spatial resolution among the points of about 1mm.

The second acquisition (2015) was performed with the structured light scanning system ATOS Compact Scan 5M produced by GOM, which consisted of a projector and two high-resolution cameras. In the second campaign, 96 range maps were acquired for the front and 111 for the back, with a few scans acquired from a side view in order to also sample the border of the painting and in order to permit the registration of the two sides. Each scan covers an area of 1100 x 900 mm with an overlap of about the 50% with each adjacent scans. The high number of scans on the front was due to the optical characteristics of some of the pigments after the painted has been cleaned, especially the darker pigments. After removing the oxidized paints, these pigments became shinier and were subsequently more challenging to acquire for the scanner. To ensure high quality data in these areas, further scans with an increasing exposure time were acquired. On the back, it was necessary to acquire more data in order to cover the undercut and small features on the surface of the panels, especially on the top and bottom sides of the crossbars - these data were partially acquired in 2002. The registration step of the range scan was simplified using several markers which could be recognized automatically by the scanner software. For the front, the markers were placed on the supporting structure around the artwork and on three metal bars which remained fixed during the acquisition in front of the painting. For the back, the targets were placed directly on the wood and on the metal braces (Figure 2). The data was processed with MeshLab [31] and produced a single 3D model for both the side composed of 65 million triangles with a spatial resolution among the sampled points of about 0.5 mm.

Both acquisition systems are based on the projection of a fringe pattern composed of multiple vertical strips with increasing resolution which, when deformed by the surface, are acquired by the camera and processed by the system in order to evaluate the geometrical shape of the surface portion framed. In the second system (ATOS), the simultaneous use of two cameras improves the precision and the accuracy of the measurements by exploiting the redundancy of the acquired data. The calculation of the 3D position is based on optical triangulation using the knowledge of the relative position of the projector and the camera obtained during the instrument's calibration.

Figure 1 shows the 3D models acquired in 2002 and in 2015 using the classical Lambertian shading with uniform color. Figure 3 shows the models using a non-

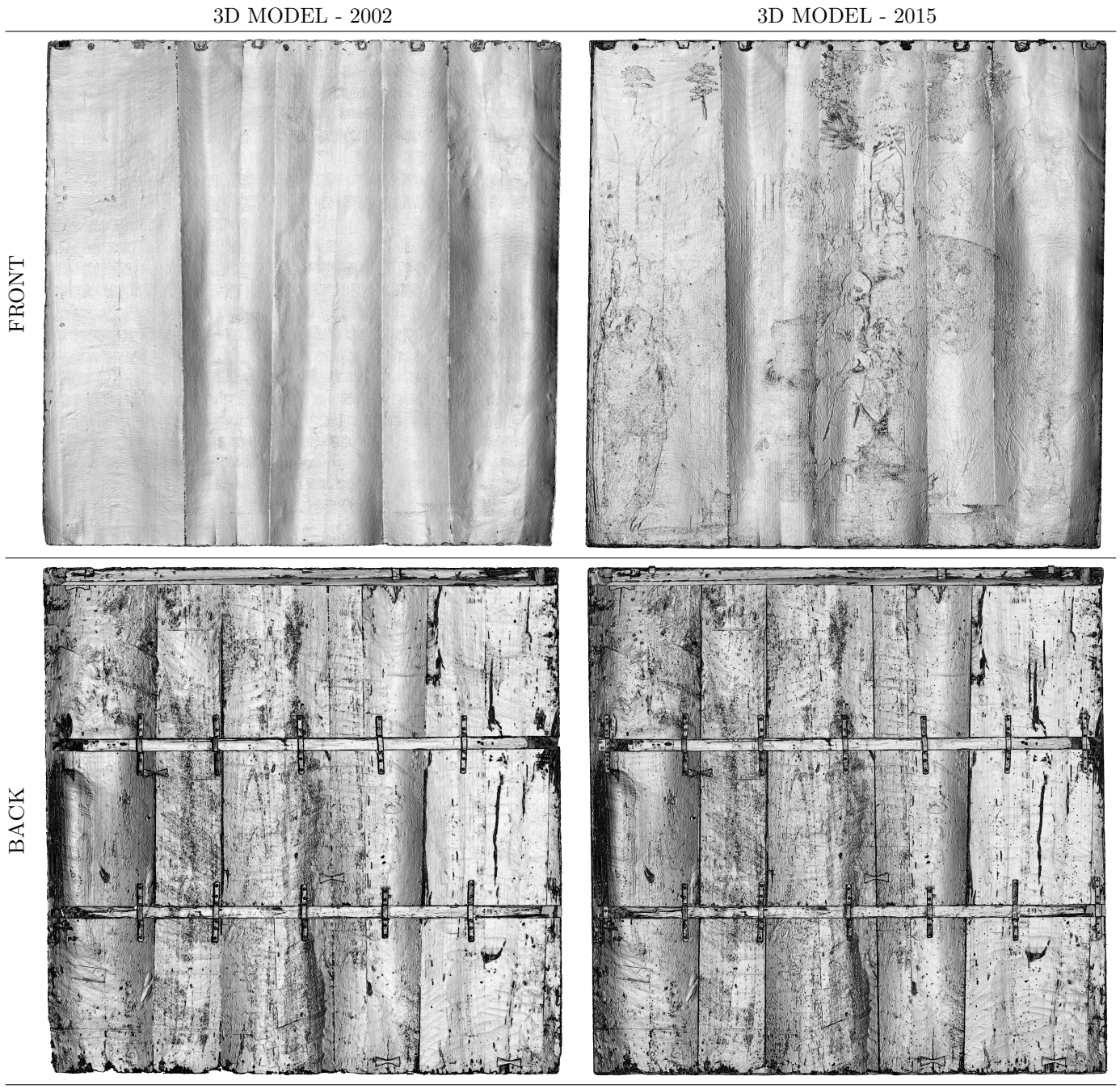

Figure 3: *Non-photorealistic rendering of the 3D models of the two sides of the "Adorazione dei Magi" using a local bending of the light direction depending on the curvature of the surfaces. The rendering emphasizes the perception of small superficial features (both real ones and scanning errors) and the curvature of the wooden support.*

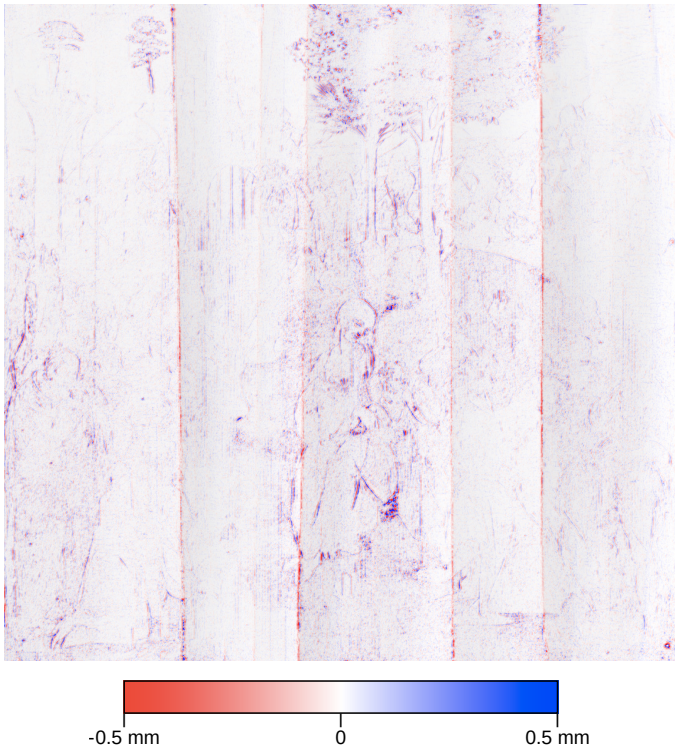

Figure 4: *Visualization of the error introduced by the scanner in the 2015 model. The figure shows the color mapping of the distance of the 2015 model from the 3D mesh filtered with the closing and opening morphological operators. This distance enables the estimation of the magnitude of the small shape imperfections (narrow ridge and valley) introduced by the scanner around the color edge with a strong color contrast. The red areas have a negative offset (valley), the blue areas have a positive offset (ridge). The maximum error is of the same order as the spatial resolution of the final model (±0.5 mm).*

photorealistic rendering technique based on a local lighting model that bends the light direction in relation of the curvature of the surface: the higher the curvature, the more grazing the light direction. This rendering thus highlights the small features on the surfaces, by exaggerating them, and thus enhances the perception of the curvature of the wooden support. On the front, the curvature and deformations of the support are better visualized, while on the back the geometrical details of the planks can be seen, such as the cracks, the woodworm holes and the cut of each plank. In addition, on the front of the 2015 model, this rendering technique highlights small shape imperfections (narrow ridge and valley) created by the scanner around the edges among the regions with high contrasting colors, such as near the border of the figure depicted with black. These errors are due to the optical characteristics of some pigments after cleaning the painted surface which become more visible for the scanner. To evaluate the errors introduced by the scanner, we computed the distance of the model from a filtered version without these small imperfections obtained with 3D mathematical morphology (Figure 4). The filtered version was computed by applying the *opening* operator (erosion followed by a dilation) to remove the concave features (narrow valley) followed by the *closing* operator (dilation followed by an erosion) to remove the convex features (narrow ridge). The structuring element used by the morphological operator is a sphere with a radius of 4 cm. This analysis revealed that the maximum error introduced by the scanner is of the same order as the spatial resolution of the final model, ±0.5 mm.

5. Geometric analysis of the 3D models

A 3D model supports the documentation and monitoring of an artwork by providing a set of analyses and geometric measurements. In the case of the "Adorazione dei Magi", the 3D models were used to measure the surface and analyse of the type of geometrical deformation of each plank. A classical way of numerically estimating this geometrical deformation is to compute the distance of the 3D model from the ideal flat plane of the painting. To permit a more robust comparison, we aligned the two models (2002 and 2015) in the same reference system with a user-assisted procedure based on two steps. The first step is the rough registration in order to compute the transformation matrix which minimizes the least square error of four pairs of corresponding points on the two models. The pairs were manually picked. The second step is to refine the computed transformation using the Iterative Closest Point (ICP) algorithm [32]. We then computed the ideal flat plane of the painting with a best fitting procedure using the data of the final model generated in 2015, excluding the points on the crossbars on the back. The computed plane is used as a common reference to estimate the deviation of the two models.

Figure 5 shows the encoding of the distance from the reference plane by mapping the distance values to a false color ramp. The distance intervals between the models and the reference plane are $[-12\text{mm}, 32\text{mm}]$ for the front of the artwork and $[-38\text{mm}, 10\text{mm}]$ for the back. Although the painting is composed of ten planks, some show a similar and continuous deformation to the adjacent ones. In fact, it is possible to identify seven vertical regions, each one characterized by a different type and magnitude of deformation. The extension of these regions is shown in Figure 5. The figure shows also the 10 planks of the support.

To numerically evaluate the evolution of the deformation over time, from 2002 to 2015, we fit a quadric surface on the data of each plank independently. In particular, given the set of points S of a plank and the quadric surface defined by the equation:

$$ax^2 + bxy + cy^2 + dx + ey + f = z \qquad (1)$$

we compute the best quadric surface for the points in S with a linear least square fitting that solves the following

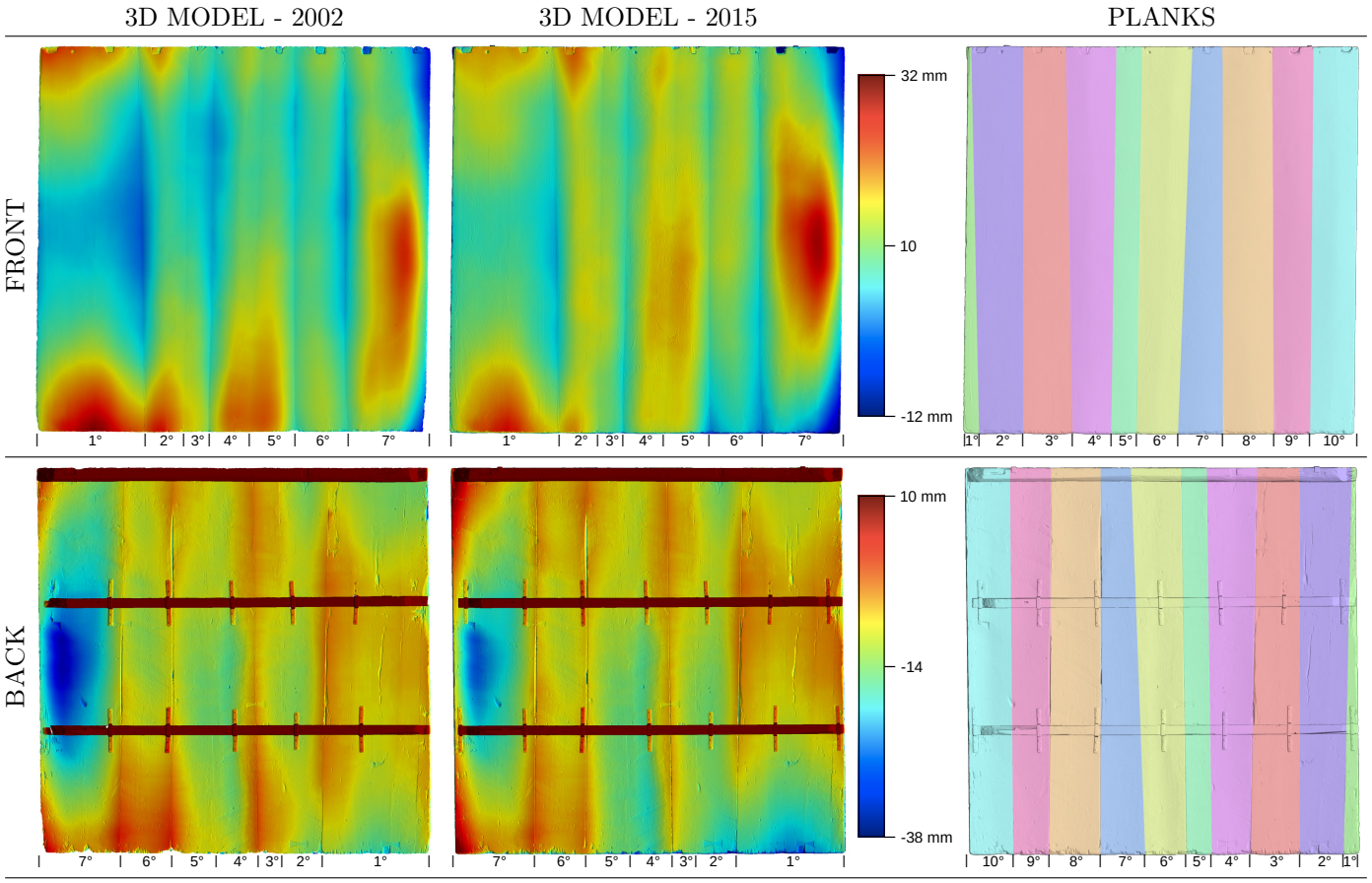

Figure 5: *Color mapping of the distance of the 3D models from the ideal flat plane of the painting. The images on the right show the subdivision of the wooden support in the ten planks. Remember that between the images of the front and of the back there is a mirror effect, so the left points of one side correspond to the right points of the other side.*

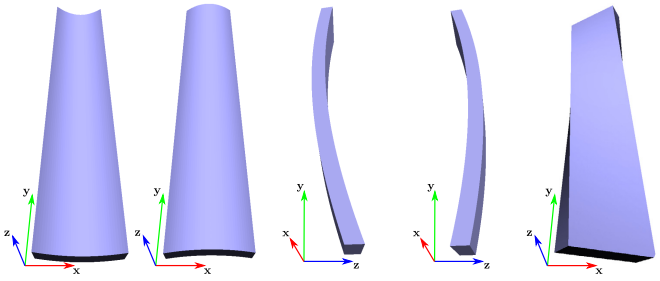

$z = x^2$ (a) $z = -x^2$ (b) $z = y^2$ (c) $z = -y^2$ (d) $z = xy$ (e)

Figure 6: *Wood warping described by a quadric surface: (a) Concave up cupping; (b) Concave down cupping; (c) Concave up bowing; (d) Concave up bowing; (e) Twisting.*

overdetermined system of linear equations:

$$\begin{bmatrix} x_0^2 & x_0y_0 & y_0^2 & x_0 & y_0 & 1 \\ x_1^2 & x_1y_1 & y_1^2 & x_1 & y_1 & 1 \\ \vdots & \vdots & \vdots & \vdots & \vdots & \vdots \\ x_n^2 & x_ny_n & y_n^2 & x_n & y_n & 1 \end{bmatrix} \begin{bmatrix} a \\ b \\ c \\ d \\ e \\ f \end{bmatrix} = \begin{bmatrix} z_0 \\ z_1 \\ \vdots \\ z_n \end{bmatrix} \quad (2)$$

where (x_i, y_i, z_i) is a point in S, and the vector $[a, b, c, d, e, f]$ contains the coefficients of the quadric surface that we want to fit. These coefficients give a measure of the different deformations on each plank. The coefficient of the quadratic term x^2 (a) returns the amount of cupping with the relative curvature direction, concave up if $a > 0$ (Figure 6a) and concave down if $a < 0$ (Figure 6b). The coefficient of the quadratic term y^2 (c) returns the amount of bowing with the curvature direction, concave up if $c > 0$ (Figure 6c) and concave down if $c < 0$ (Figure 6d). Instead, the coefficient of the term xy (b) returns the amount of twisting (Figure 6e). The last three coefficients d, e and f only affect the position of the stationary point of the quadric surface. For the values to be comparable between the different deformation directions, the x and y coordinates of the points in each plank are translated in the centroid of the plank and scaled in the range $[-0.5, 0.5]$ using the size of the bounding box of the plank.

Table 1 contains the coefficients of the quadric surface for each plank for the front surface of the 2002 and 2015 models. The further the coefficients a, b and c are from zero, the greater deformation. The table also contains the Root Mean Square Error (RMSE) and the Mean Absolute Error (MAE) of the quadric surface with respect to the original data in millimeters in order to provide information on the accuracy of the fitting procedure. The residual errors are very low with values around 1mm.

From a careful analysis of the coefficients of the quadric surfaces, an evolution can be seen from left to right of the bowing deformation from a concave up to a concave down (coefficient c). On the other hand, the cupping deformation is always concave down with different amounts for the different planks (coefficient a). With the exception of the first plank which is very narrow, the tenth plank shows the largest cupping while the central planks present a more limited deformation. The magnitude of the twisting deformation changes among the planks, with the highest score in the fifth and seventh planks. Analyzing the data over reveals that between 2002 and 2015 the cupping was almost stable (the differences in the coefficient a are very small). The only exceptions are the first and tenth planks where the cupping increases in 2015 due to the new metal braces added on the side of the crossbars during the last restoration (see Figure 12). Conversely, the changes in the bowing are more substantial. The first six planks of 2015 show a lower bowing (the coefficient c is closer to zero in 2015), while the last four planks show a higher deformation. The point of change in the curvature direction, from concave up to concave down, also moves from the last plank in 2002 to the fifth plank in 2015. For the twisting,

Plank 1	a	b	c	d	e	f	RMSE	MAE
2002	-29.05	-7.66	60.52	12.26	-6.18	-4.70	0.91	0.72
2015	-40.59	-7.71	32.61	11.63	-5.82	-2.16	0.70	0.50
Plank 2	a	b	c	d	e	f	RMSE	MAE
2002	-2.74	-8.98	70.63	0.37	2.83	-5.90	0.87	0.72
2015	-2.31	-4.77	43.01	1.27	-0.95	-3.36	0.78	0.61
Plank 3	a	b	c	d	e	f	RMSE	MAE
2002	-1.44	0.97	68.40	-6.67	-4.10	-5.76	0.55	0.48
2015	-1.41	5.27	41.30	-6.23	-3.41	-3.28	0.58	0.48
Plank 4	a	b	c	d	e	f	RMSE	MAE
2002	-21.24	-9.35	44.37	4.34	-1.41	-2.07	1.22	1.02
2015	-22.38	-5.99	17.52	5.47	2.16	0.26	1.31	1.06
Plank 5	a	b	c	d	e	f	RMSE	MAE
2002	-18.68	10.89	22.10	-7.61	-5.80	-1.53	0.93	0.74
2015	-18.68	10.18	-5.26	-8.30	0.99	0.83	0.82	0.66
Plank 6	a	b	c	d	e	f	RMSE	MAE
2002	-12.73	0.22	24.43	7.24	-7.61	-1.08	0.80	0.63
2015	-13.62	0.54	-0.70	7.92	-2.08	1.17	0.78	0.63
Plank 7	a	b	c	d	e	f	RMSE	MAE
2002	-18.35	11.19	9.88	-6.49	-9.78	-0.006	0.79	0.64
2015	-18.84	12.03	-15.83	-7.19	-0.06	2.22	0.71	0.56
Plank 8	a	b	c	d	e	f	RMSE	MAE
2002	-15.55	2.31	15.08	-2.47	-2.59	0.15	0.91	0.71
2015	-15.38	1.51	-12.41	-2.55	6.05	2.50	0.71	0.56
Plank 9	a	b	c	d	e	f	RMSE	MAE
2002	-19.10	-6.12	2.21	11.58	-3.92	0.91	1.25	0.95
2015	-19.04	-6.51	-28.37	11.39	4.75	3.42	1.22	0.94
Plank 10	a	b	c	d	e	f	RMSE	MAE
2002	-26.06	3.08	-50.51	-11.83	-7.87	6.46	1.77	1.42
2015	-27.99	2.65	-82.13	-12.66	1.97	8.80	1.67	1.31

Table 1: *Coefficients of the quadric surfaces fitted on the points of each plank of the support for the 2002 and 2015 models. The table also shows the residual fitting error computed as Root Mean Square Error(RMSE) and Mean Absolute Error(MAE).*

the magnitude of the deformation remains constant over time with the exception of the second and fourth planks, where it is less in 2015, and the third plank, where it is increased in 2015.

6. Temporal Comparison

A simple way to estimate the deformation occurring over time is to compute the point-to-mesh distance between the two models. For each point of one model, we look for the closest point in the other model. This procedure gives us only a rough estimation of the real deformation because it creates misleading correspondences between the points (the closest point is not the corresponding point). To obtain a more robust estimation of the deformation occurring in the 13 years elapsed between the 3D acquisitions, we devised a new approach based on a non-rigid registration procedure that deforms the 2002 model over the 2015 model. The general idea is to compute a shape transformation encoded as a generic function in between an exact mapping of the 3D models and a rigidity-preserving mapping. We used the non-rigid registration method proposed in [33] which facilitates the registration of meshes made of tens of millions of triangles in a few minutes. The estimated non-rigid deformation can be used to compute the exact match between the points of the two models and estimate the real displacement vector between them.

Given two triangular meshes A (2015 model) and B (2002 model), the goal of the algorithm is to align B over A, when B also exhibits a deformation that cannot be modeled with a single rigid transformation. The method starts with a decomposition of B into smaller patches with a Voronoi clustering. This decomposition is used to build the topology of a deformation graph as the dual graph of the clustering. It then aligns each patch of B with A using an ICP algorithm to estimate a local rigid transformation to store in each node of the deformation graph. During this computation, the algorithm imposes some geometric constraints to guarantee a smooth deformation between adjacent patches. In particular, if the patch is too flat the algorithm extends the patch with the adjacent ones until it reaches a good normal distribution. Then if the estimation is of a low quality or if there is sliding between the surfaces, the algorithm recomputes the estimated transformation using the transformations of the adjacent patches. Finally, the algorithm computes a global deformation function that locally blends the finite set of estimated transformations at the nodes of the deformation graph. This global function is used to estimate the final deformation for each point of B. This procedure is iterated using the output of the previous iteration as input until convergence. In each iteration, the algorithm quadruples the number of patches in the clustering and divides by four the maximum amount of displacement that each patch is allowed during the ICP procedure. The evolution of the two parameters captures smaller deformations. This strategy is well known and used in several non-rigid registration algorithms, such as [34] where it was proposed for the first time. For the input models we use three iterations with 100, 400 and 1600 patches (shown in Figure 7), starting from a maximum initial displacement of $48mm$ (the range of the displacement from the ideal flat panel computed in Section 5 and visible in Figure 5). The two parameters (number of patches and maximum displacement) prevent real changes in the surface from being embedded in the computed deformation. The method could destroy changes of the same size such as the portion of the surface used in the ICP step of the algorithm. In our case, the use of a multi-resolution approach with a decreasing maximum displacement for each patch, which moves the surface of the model towards the reference of a limited amount, avoids this problem. For more details on the non-rigid registration algorithm see [33]. This method requires an initial rough alignment of the two meshes. We use the same procedure described in Section 5. Figure 8 shows the initial alignment between the two models (left) and the final alignment after the non-rigid registration algorithm (right).

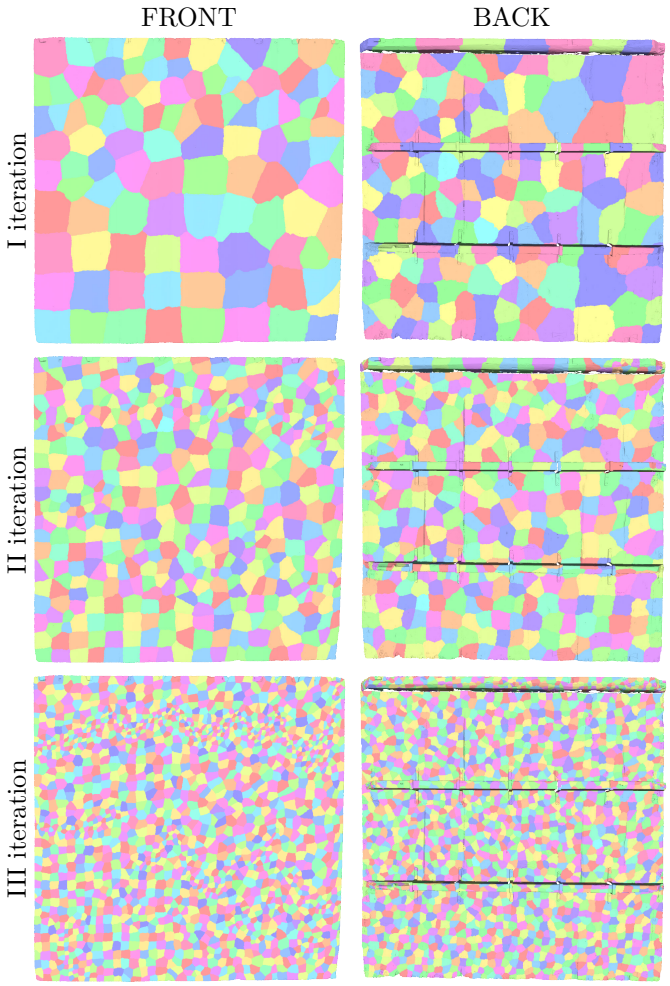

Figure 7: *Patch decomposition of the 2002 models during the three iterations of the non-rigid registration algorithm: I iteration 100 patches; II iteration 400 patches; III iteration 1600 patches*

After the non-rigid registration, we have three models:

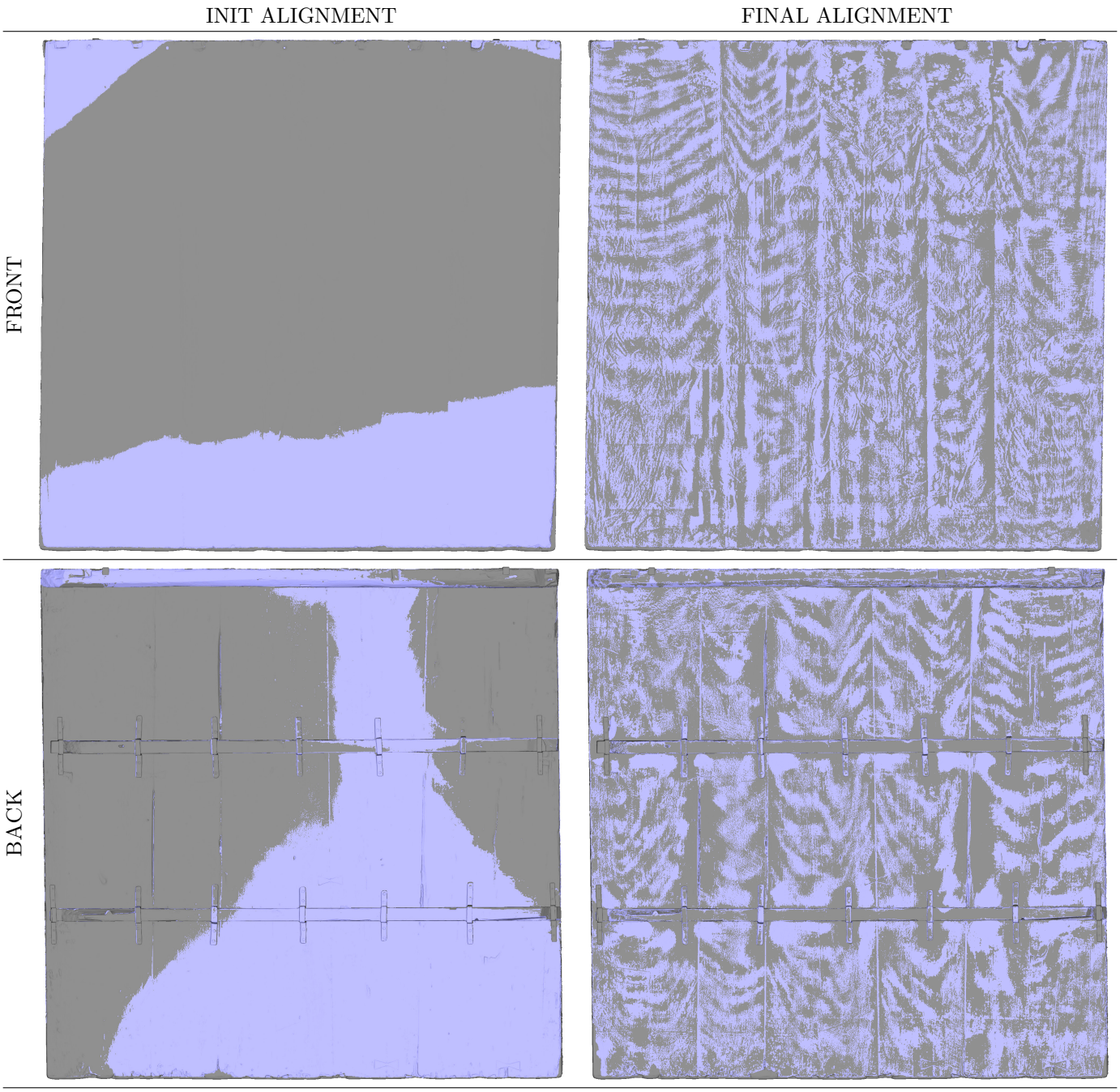

Figure 8: *Alignment results between the two models. The grey model is the fixed reference model (2015). The violet model is the deformed one (2002). (Left) Initial alignment obtained with the manual picking of 4 pairs of corresponding points followed by an ICP refinement. (Right) Final non-rigid registration after the algorithm described in [33].*

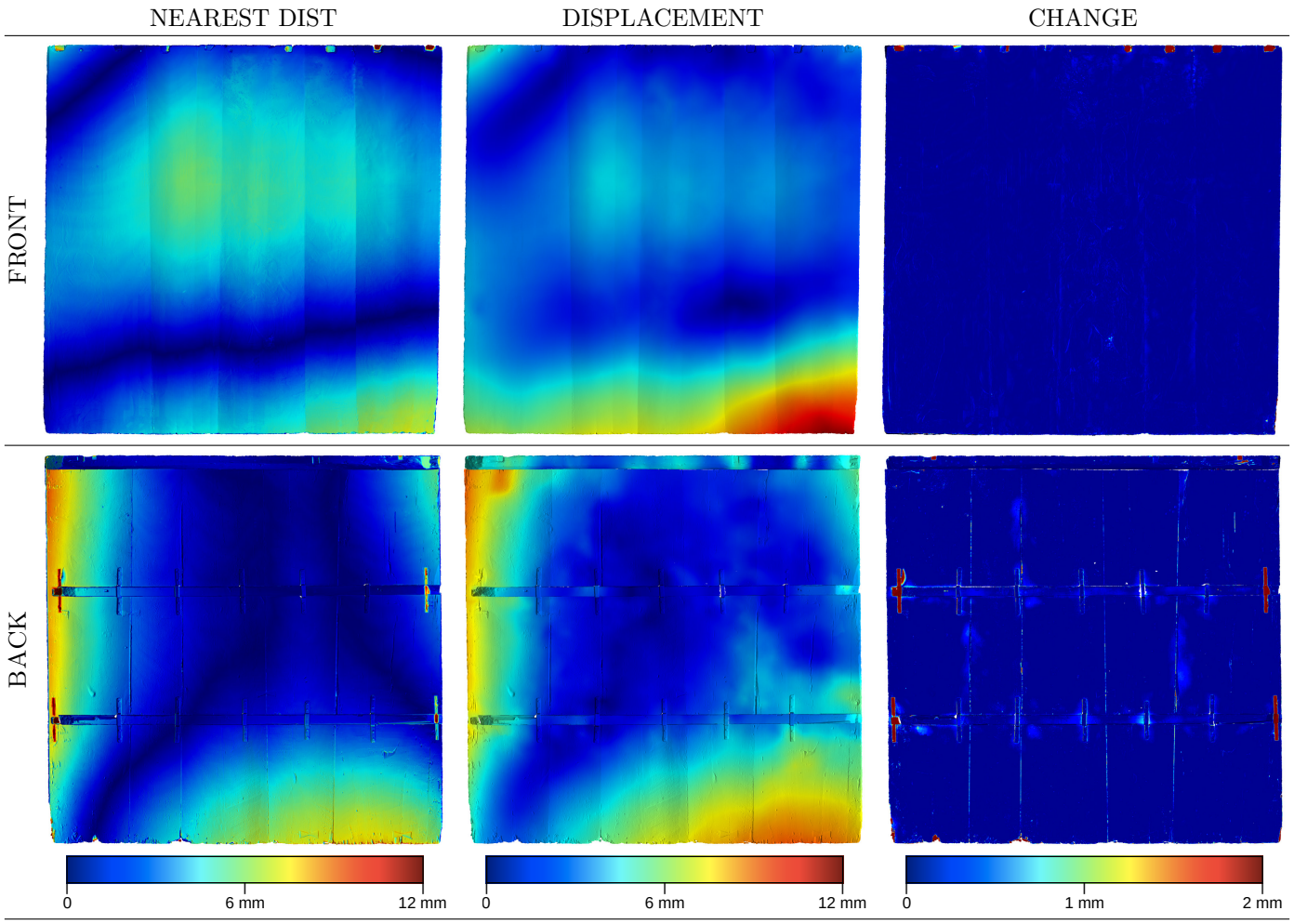

Figure 9: *Information extracted from the models before and after the non-rigid registration of the two models (2015 and 2002). The first column shows the absolute value of the point-to-mesh distance between the 2015 model and the 2002 model. The second column shows the real deformation displacement by computing the absolute distance between a point in the 2002 model and the same point after the non-rigid deformation. The third column shows the point-to-mesh absolute distance between the 2015 model and the deformed version of the 2002 model. The last two columns separate the contribution of the panel deformation from the structural changes introduced by the restorations. Remember that between the images of the front and of the back there is a mirror effect, so the left points of one side correspond to the right points of the other side.*

2015 (A), 2002 (B) and the deformed 2002 (C). Using all this data, we can extract more information on the deformation and the structural changes of the wooden panel of the artwork. The simplest solution is to compute the point-to-mesh distance between B and A, by looking for the closest point on A for each point of B and computing the distance between these points. The left column in Figure 9 shows a color mapping of the absolute value of this distance. It gives some information on the deformation however it is not able to separate the real deformation of the wooden panel from the structural changes introduced by the different restorations, such as the additional braces on the side of the crossbar on the back. This happens when the change is of the same order as the panel deformation, for example on the sides of the artwork.

A more robust analysis is possible by comparing the deformed model C with the other models. We can estimate the real displacement of each point of model B by computing the displacement vector as the difference between a point of model C after the deformation and the same point in the original model B. A color mapping of the magnitude of this displacement vector field is shown in the central column of Figure 9. The figure proves that the simple point-to-mesh distance between A and B underestimates the entity of the deformation, especially on the side of the artwork. Another interesting information to visualize of this vector field is the displacement direction. Figure 10 shows this deformation fields with a set of 3D arrows. To avoid a cluttered visualization, we sampled the deformation field in an adaptive way to extract a limited number of vectors denser in the areas with less deformation. The size and the length of each arrow are proportional to the magnitude of the vector; the bigger the displacement, the longer and the bigger the arrow. To improve the understanding of the deformation we multiplied the displacement by a factor 20×. Figure 10 visualizes

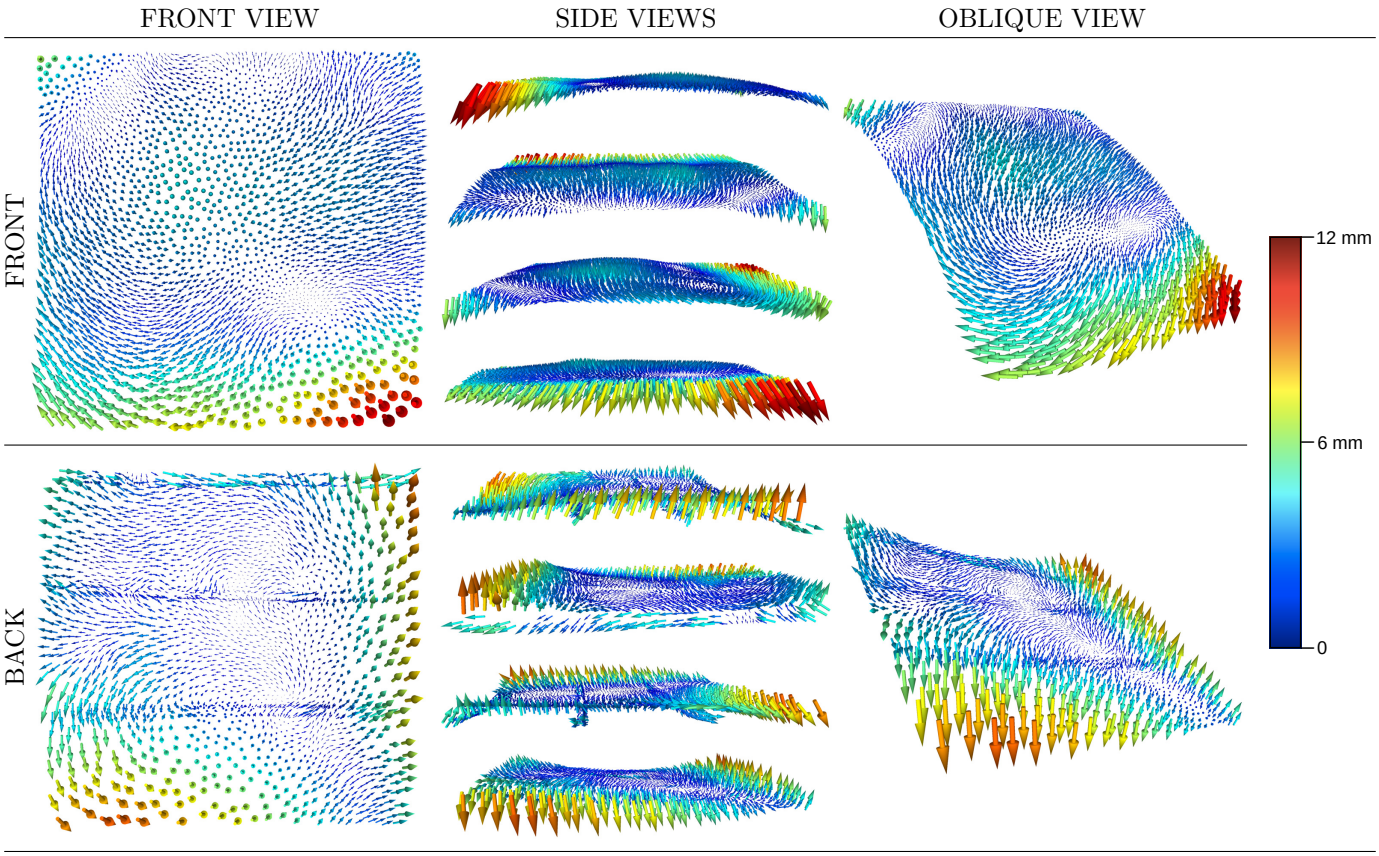

Figure 10: *Visualization of the displacement vectors computed between the deformed version of the 2002 model after the non-rigid registration and the original 2002 model. Direct visualization of sampled displacement vectors shown as 3D arrows colored with the magnitude of the displacement. For each side, there is the frontal view, the side views (right, top, left and bottom) and an oblique view of the vector field. To improve the perception of the deformation we increased the magnitude by a factor* $20\times$.

the vector from different viewpoints: the front view (left column); the four side views right, top, left and bottom (central column); an oblique view. Analyzing this visual data, the deformation was reduced from 2002 to 2015, especially the bowing.

The computation of the point-to-mesh distance between A and C also highlights the structural changes due to the restoration. This is possible because the smooth deformation computed by the non-rigid registration algorithm preserves these kinds of changes. This distance is shown in the right column in Figure 9. We can also evaluate the residual alignment error introduced by the non-rigid registration procedure. The residual is below the highest spatial resolution of the two models (1mm) with the exception of the area with structural changes.

Finally, Figures 11 and 12 show a segmentation of the areas with the most significant structural changes obtained by selecting all the points in the model B with a distance from the deformed version C greater than 1 mm (the spatial resolution of the 2002 model). For each area, a magnification highlights the changes. On the front, the main changes are related to the cut pieces of wood on the top, which were moved during the monitoring period, and some nails (regions a, b, d and f in Figure 11) on the top which in 2015, at the time of the 3D scanning, were temporally removed for the restoration. On the back, the main changes are the wooden support on the top of the highest crossbar (regions a and b in Figure 12), some lost pieces of wood (region b in Figure 12), and the side braces on the two central crossbars (regions c, d, e and f in Figure 12). The changes detected in the bottom right corner of the front (region i in Figure 11) and in the bottom border of the back (regions g, h and i in Figure 12) are due to maintenance in 2002 after the 3D acquisition, where some eroded areas of the support were reconstructed with old poplar. This maintenance works are also confirmed by the color image of the front and back (first column in Figure 1).

7. Conclusion

The paper presents an innovative approach to estimate the deformations of a panel painting over time, obtained by comparing 3D models acquired with different scanning devices in different years. The proposed method was tested on the unfinished panel painting “Adorazione dei Magi” by Leonardo da Vinci, with data acquired in 2002 and

2015. After a description of the two 3D scanning campaigns, highlighting the features and the limitations of the acquisition devices, we applied a series of geometric analyses on the acquired data to produce numerical and visual evidence of the deformation. First, we analyzed the two 3D models with the classical distance from the ideal flat plane. Then we identified the type and amount of deformations for each plank of the wooden support by fitting a quadric surface on its geometric data and analyzing the trend of the most significant coefficients of the fitted function. Finally, we compared the 3D models in a more robust way using a non-rigid registration algorithm which deforms the 2002 model over the 2015 model. Comparing the deformed model with the other models, it is possible to extract more interesting information. We can separate the real low-frequency deformation of the wooden support from the structural changes in a robust way, such as the structural restoration on the back (the additional metal braces on the side of the crossbars and the integrated missing parts on the bottom) or the missing wooden parts on the top of the back. The results presented in this paper were used to decide on new structural modifications of the support during the last restoration phase after 2015. The restores and conservators decided to restore the fourth crossbar at the bottom of the support and to modify the existing three crossbars in order to reduce the stress on the ten planks. These results were then used to document the temporal evolution of the support's deformation. To note that, while the analyses based on the distance from the flat plane and on the quadric surface fitting are tailored for objects with an almost planar surface, for example a panel painting, the last contribution based on the non-rigid registration can be generalized for objects of any shape. A future work direction is to use the output of the non-rigid registration procedure, capturing also more than two models, to estimate a mathematical model of the object's deformation which can be used to predict its changes.

References

[1] M. Ciatti, C. Frosinini, Il restauro dell'Adorazione dei Magi di Leonardo, Edifir, 2017.

[2] C. Castelli, A. Santacesaria, La struttura lignea dell'adorazione. vicende conservative e restauro di un supporto costruito a risparmio., in: M. Ciatti, C. Frosinini (Eds.), Il restauro dell'Adorazione dei Magi di Leonardo. La riscoperta di un capolavoro, Edifir, 2017, pp. 191–202.

[3] A. van Grevenstein, B. New, C. Young, K. Seymour, R. Groves, V. Horie, The conservation of panel paintings and related objects, Netherlands Organisation for Scientific Research, 2014.

[4] R. G. Maev, D. Gavrilov, A. Maeva, I. Vodyanoy, Modern nondestructive physical methods for paintings testing and evaluation, in: 9th International Conference on NDT of Art, 2008, pp. 1–13.

[5] M. Elias, N. Mas, P. Cotte, Review of several optical nondestructive analyses of an easel painting. Complementarity and crosschecking of the results, Journal of Cultural Heritage 12 (4) (2011) 335 – 345.

[6] S. Sfarra, P. Theodorakeas, C. Ibarra-Castanedo, N. P. Avdelidis, A. Paoletti, D. Paoletti, K. Hrissagis, A. Bendada, M. Koui, X. Maldague, Importance of integrated results of different non-destructive techniques in order to evaluate defects in panel paintings: the contribution of infrared, optical and ultrasonic techniques, Proc.SPIE 8084 (2011) 8084 – 8084 – 13.

[7] D. Ambrosini, D. Paoletti, G. Galli, Integrated digital speckle based techniques for artworks monitoring, in: Lasers in the Conservation of Artworks - Proceedings of the International Conference LACONA 7, CRC Press, 2008, pp. 399–405.

[8] R. Groves, B. Pradarutti, E. Kouloumpi, W. Osten, G. Notni, 2D and 3D non-destructive evaluation of a wooden panel painting using shearography and terahertz imaging, NDT & E International 42 (6) (2009) 543 – 549.

[9] K. Janssens, J. Dik, M. Cotte, J. Susini, Photon-based techniques for nondestructive subsurface analysis of painted cultural heritage artifacts, Accounts of Chemical Research 43 (6) (2010) 814–825.

[10] L. Senni, C. Casieri, A. Bovino, M. C. Gaetani, F. De Luca, A portable NMR sensor for moisture monitoring of wooden works of art, particularly of paintings on wood, Wood Science and Technology 43 (1) (2009) 167–180.

[11] D. Gavrilov, C. Ibarra-Castanedo, E. Maeva, O. Grube, X. Maldague, R. Maev, Infrared methods in noninvasive inspection of artwork, in: 9th International Conference on NDT of Art, Jerusalem, Israel, 2008, pp. 1–5.

[12] A. Casini, F. Lotti, M. Picollo, L. Stefani, E. Buggezzoli, Image spectroscopy mapping technique for non-invasive analysis of paintings, Studies in Conservation 44 (1) (1999) 39–48.

[13] G. Guidi, C. Atzeni, M. Seracini, S. Lazzari, Painting survey by 3D optical scanning - The Case of Adoration of the Magi by Leonardo Da Vinci, Studies in Conservation 49 (1) (2004) 1–12.

[14] D. Abate, F. Menna, F. Remondino, M. G. Gattari, 3D painting documentation: evaluation of conservation conditions with 3D imaging and ranging techniques, ISPRS - International Archives of the Photogrammetry, Remote Sensing and Spatial Information Sciences (2014) 1–8.

[15] F. Remondino, A. Rizzi, L. Barazzetti, M. Scaioni, F. Fassi, R. Brumana, A. Pelagotti, Review of geometric and radiometric analyses of paintings, The Photogrammetric Record 26 (136) (2011) 439–461.

[16] R. Fontana, M. C. Gambino, M. Greco, L. Marras, M. Materazzi, E. Pampaloni, L. Pezzati, P. Poggi, Integrating 2D and 3D data for diagnostics of panel paintings, in: Proc. SPIE, Vol. 5146, 2003, pp. 5146 – 5146 – 11.

[17] A. Pelagotti, A. D. Mastio, A. D. Rosa, A. Piva, Multispectral imaging of paintings, IEEE Signal Processing Magazine 25 (4) (2008) 27–36.

[18] M. Manfredi, G. Bearman, G. Williamson, D. Kronkright, E. Doehne, M. Jacobs, E. Marengo, A new quantitative method for the non-invasive documentation of morphological damage in paintings using rti surface normals, Sensors (Basel, Switzerland) 14 (7) (2014) 12271–12284.

[19] S. Robson, S. L. Bucklow, N. M. J. Woodhouse, H. A. Papadaki, Periodic photogrammetric monitoring and surface reconstruction of a historical wood panel painting for restoration purposes, in: International Society for Photogrammetry and Remote Sensing Archives, Vol. XXXV, 2004, pp. 395 – 400.

[20] Ł. Bratasz, S. Jakieła, R. Kozłowski, Allowable thresholds in dynamic changes of microclimate for wooden cultural objects: monitoring in situ and modelling, James & James, Earthscan, London, 2005.

[21] A. Brewer, C. Forno, Moiré fringe analysis of cradled panel paintings, Studies in Conservation 42 (4) (1997) 211–230.

[22] G. Schirripa Spagnolo, R. Majo, D. Ambrosini, D. Paoletti, Digital moiré by a diffractive optical element for deformation analysis of ancient paintings, Journal of Optics A: Pure and Applied Optics 5 (2003) S146–S151.

[23] F. Brémand, P. Doumalin, J.-C. Dupr, F. Hesser, V. Valle, Relief analysis of the Mona Lisas wooden panel, in: Proceedings of the XIth International Congress and Exposition. Orlando, Florida USA, Society for Experimental Mechanics Inc, 2008, pp. 1 – 8.

[24] Ł. Lasyk, M. Łukomski, T. M. Olstad, A. Haugen, Digital speckle pattern interferometry for the condition surveys of painted wood: Monitoring the altarpiece in the church in Hedalen, Norway, Journal of Cultural Heritage 13 (3, Supplement) (2012) S102 – S108, wood Science for Conservation.

[25] E. Bernikola, A. Nevin, V. Tornari, Rapid initial dimensional changes in wooden panel paintings due to simulated climate-induced alterations monitored by digital coherent out-of-plane interferometry, Applied Physics A 95 (2) (2009) 387–399.

[26] C. R. Young, M. Debashis, Using ESPI to characterise the mechanical behaviour of paintings on canvas, in: 12th International User EPSI Group Meeting, 2005.

[27] T. Olstad, A. Haugen, Warm feet and cold art: is this the solution? Polychrome wooden ecclesiastical art - Climate and dimensional changes, Museum Microclimates, National Museum of Denmark (2007) 43–49.

[28] P. Dionisi-Vici, P. Mazzanti, L. Uzielli, Mechanical response of wooden boards subjected to humidity step variations: Climatic chamber measurements and fitted mathematical models, Journal of Cultural Heritage 7 (2006) 37 – 48.

[29] G. Sansoni, M. Carocci, R. Rodella, Three-dimensional vision based on a combination of gray-code and phase-shift light projection: Analysis and compensation of the systematic errors, Applied optics 38 (1999) 6565–6573.

[30] PolyWorks (2018).
URL `https://www.innovmetric.com/`

[31] P. Cignoni, M. Callieri, M. Corsini, M. Dellepiane, F. Ganovelli, G. Ranzuglia, MeshLab: an Open-Source Mesh Processing Tool, in: V. Scarano, R. D. Chiara, U. Erra (Eds.), Eurographics Italian Chapter Conference, The Eurographics Association, 2008, pp. 129–136.

[32] P. J. Besl, N. D. McKay, A method for registration of 3-D shapes, IEEE Transactions on Pattern Analysis and Machine Intelligence 14 (2) (1992) 239–256.

[33] G. Palma, T. Boubekeur, F. Ganovelli, P. Cignoni, Scalable non-rigid registration for multi-view stereo data, ISPRS Journal of Photogrammetry and Remote Sensing 142 (2018) 328–341.

[34] H. Li, R. W. Sumner, M. Pauly, Global correspondence optimization for non-rigid registration of depth scans, Computer Graphics Forum 27 (5) (2008) 1421–1430.

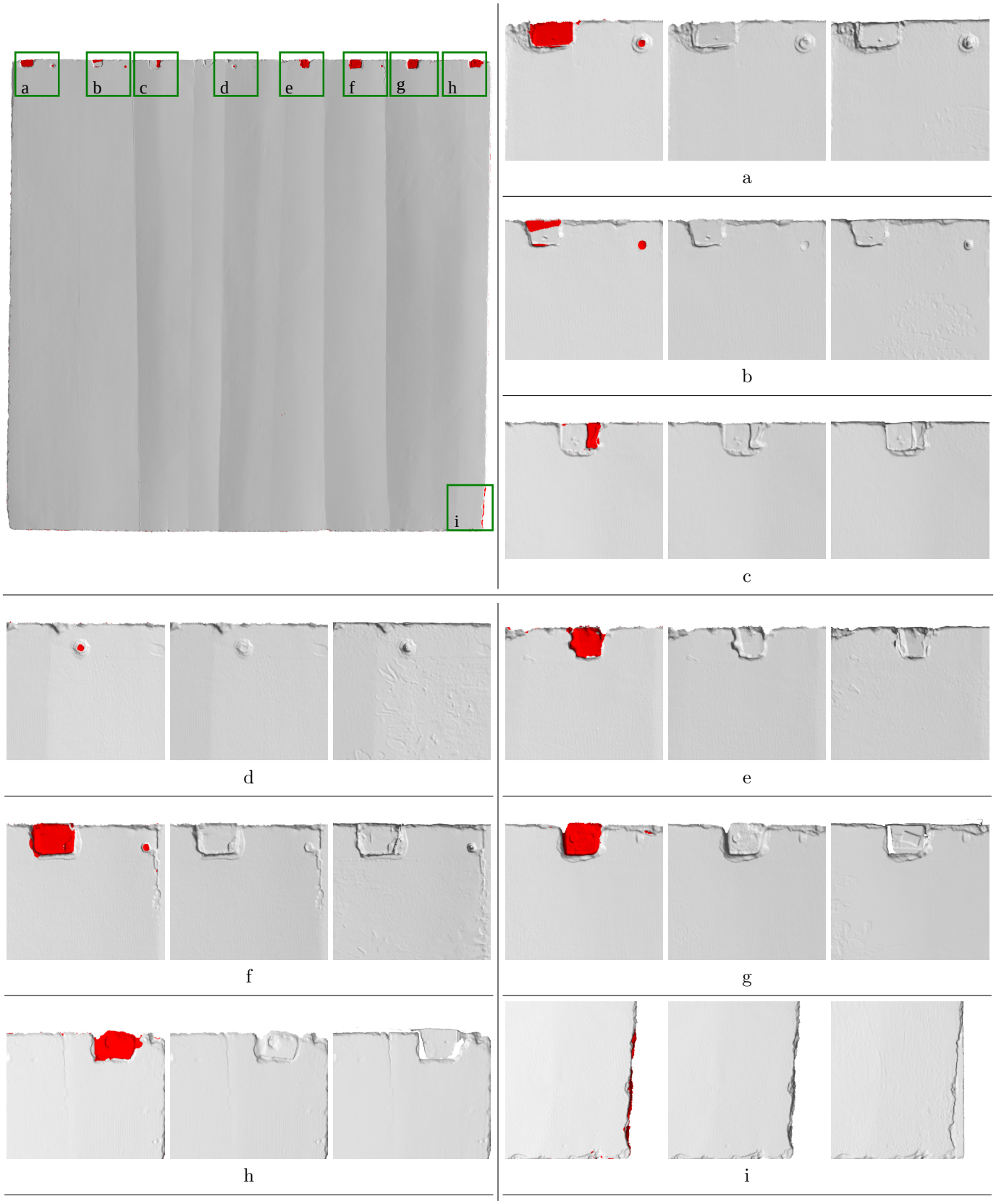

Figure 11: *Map of the structural changes of the front occurring from 2002 to 2015. The map shows all the changes greater than 1mm. For each changed area, a magnification shows the map and the two models in order to better highlight the changes: (left) change map, (center) 2002 model, (right) 2015 model.*

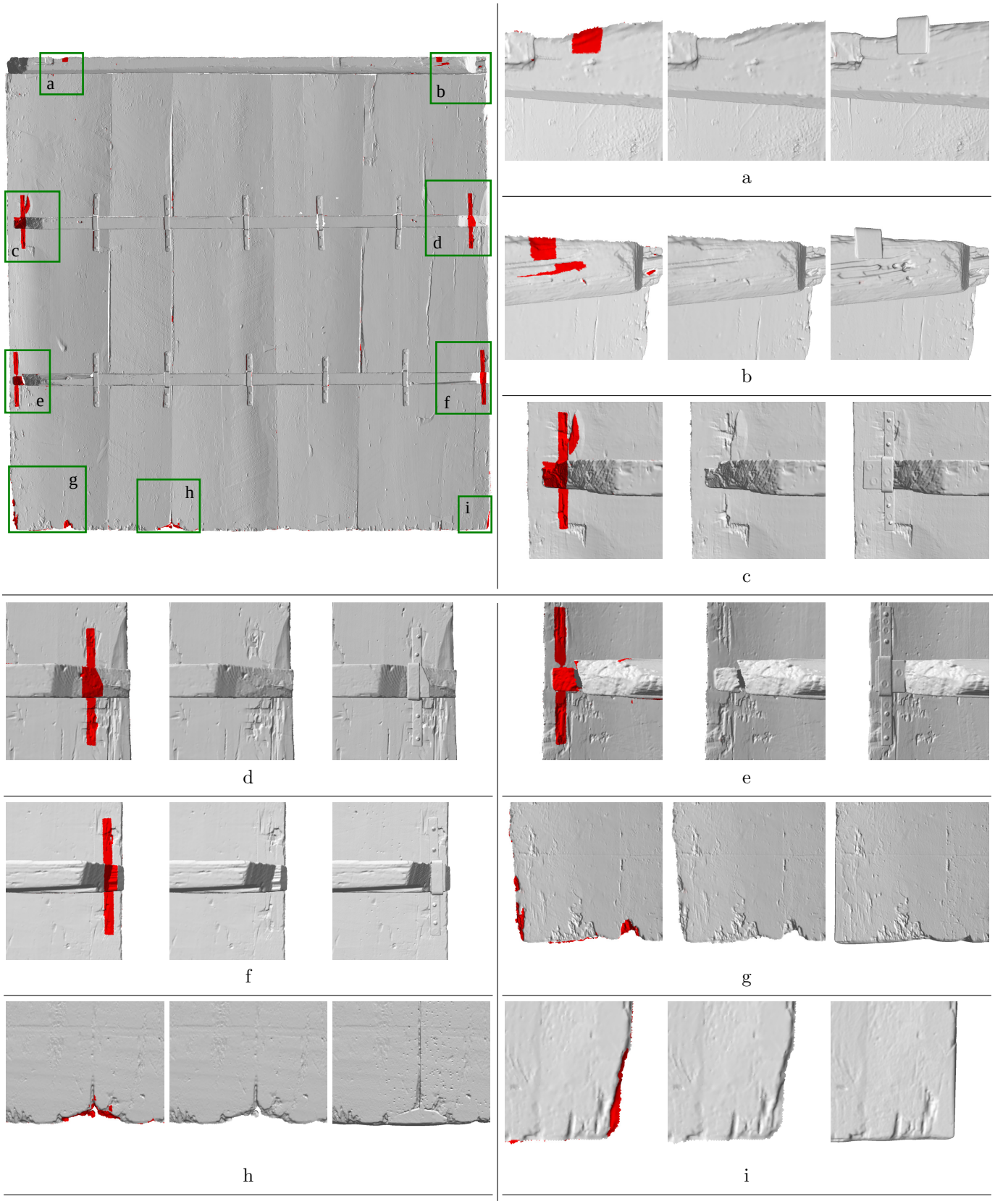

Figure 12: *Map of the structural changes of the back occurring from 2002 to 2015. The map shows all the changes greater than 1mm. For each changed area, a magnification shows the map and the two models in order to better highlight the changes: (left) change map, (center) 2002 model, (right) 2015 model.*